

# Localization properties of Dirac modes at the Roberge-Weiss phase transition

Marco Cardinali,<sup>1,\*</sup> Massimo D’Elia,<sup>1,†</sup> Francesco Garosi,<sup>2,‡</sup> and Matteo Giordano<sup>3,§</sup>

<sup>1</sup>*Dipartimento di Fisica dell’Università di Pisa and INFN - Sezione di Pisa, Largo Pontecorvo 3, I-56127 Pisa, Italy*

<sup>2</sup>*SISSA, Via Bonomea 265, 34136, Trieste, Italy*

<sup>3</sup>*ELTE Eötvös Loránd University, Institute for Theoretical Physics, Pázmány Péter sétány 1/A, H-1117, Budapest, Hungary*

We study the localization properties of the low-lying Dirac eigenmodes in QCD at imaginary chemical potential  $\hat{\mu}_I = \pi$  at temperatures above the Roberge-Weiss transition temperature  $T_{RW}$ . We find that modes are localized up to a temperature-dependent “mobility edge” and delocalized above it, and that the mobility edge extrapolates to zero at a temperature compatible with  $T_{RW}$ . This supports the existence of a strong connection between localization of the low Dirac modes and deconfinement, studied here for the first time in a model with a genuine deconfinement transition in the continuum limit in the presence of dynamical fermions.

## I. INTRODUCTION

The interest in gauge theories at nonzero imaginary chemical potential is due both to practical and theoretical reasons. On the one hand, they are a means to side-step the notorious sign problem encountered at real chemical potential: being free from the sign problem, they allow direct numerical simulations with importance sampling methods, from which one can attempt an analytic continuation to the physically relevant case of real chemical potential [1–17]. On the other hand, they provide an interesting testing ground to study the interplay of dynamical fermions and the center symmetry of the pure gauge theory, and how this affects the phase diagram of the theory.

As is well known, the analogue of center symmetry in the case of  $SU(N_c)$  theories with dynamical fundamental fermions is the Roberge-Weiss symmetry [18], that states that the partition function is periodic in the reduced imaginary chemical potential  $\hat{\mu}_I = \mu_I/T$  with period  $2\pi/N_c$ . This periodicity is realized differently at low and at high temperatures: while analytic in  $\hat{\mu}_I$  at low  $T$ , at high  $T$  the partition function displays lines of first order phase transitions at  $\hat{\mu}_I = (2k + 1)\pi/N_c$ . These transitions correspond to a change in the center sector favored by the fermions. The RW transition lines and their endpoints have been thoroughly investigated by lattice simulations [1, 2, 6, 19–37] and effective models [38–50]. Depending on the value of the quark masses, the first order lines end at a second-order point at  $T_{RW}$ , or alternatively at a triple point, which is connected via a (pseudo)critical line to the (pseudo)critical temperature at vanishing chemical potential.

A growing body of evidence indicates that center symmetry is intimately related also with another aspect of the physics of fermions that changes radically as the system transitions to the high temperature phase, namely

the localization properties of the low-lying eigenmodes of the Dirac operator (see Ref. [51] for a recent review). It has been shown in a rather large variety of gauge theories, including QCD, that as the theory crosses over from the confined to the deconfined phase, the low Dirac modes turn from delocalized to localized, up to a “mobility edge”  $\lambda_c$  in the spectrum, above which they are again delocalized [52–68]. The strong connection observed between localization and deconfinement is clarified by the mechanism provided by the “sea/islands picture” of localization proposed in Refs. [69–72]. This picture relates localized modes with local fluctuations of the Polyakov loop away from its ordered value (i.e., 1) in the high-temperature phase, which provide “energetically” favorable locations for the fermions. Numerical support for this picture has been obtained in various cases [62, 63, 68, 69].

Since in QCD the transition is an analytic crossover, the statement that localization of the low modes and deconfinement happen together can only be of qualitative nature. Localization in the presence of a sharp transition has been mostly investigated in pure gauge theories, selecting the “physical” center sector (i.e., real positive expectation value of the Polyakov loop) in the spontaneously broken phase. In these cases localization and deconfinement have been shown to coincide within numerical uncertainties [64–68]. The only study with dynamical fermions and a genuine phase transition is that of Ref. [61], concerning the  $SU(3)$  theory in the presence of unimproved staggered fermions on coarse lattices, where again localization was found to appear exactly at the transition. However, while this model is well defined as a statistical system on the lattice, the transition is known to be only a lattice artifact [73–75].

An interesting and as yet unexplored scenario is that of a genuine phase transition in the presence of dynamical fermions that survives the continuum limit. The Roberge-Weiss transition precisely provides such a scenario. In fact, the imaginary chemical potential effectively modifies the “twist” imposed on the Dirac modes by the antiperiodic boundary conditions, and favors configurations where the Polyakov loops most effectively

\* marco.cardinali@pi.infn.it

† massimo.delia@unipi.it

‡ fgarosi@sissa.it

§ giordano@bodri.elte.hu

“neutralize” it. For gauge group  $SU(3)$  and  $\hat{\mu}_I = \pi$ , these correspond to the two complex sectors  $e^{\pm i\frac{2\pi}{3}}$ , which leaves an exact  $\mathbb{Z}_2$  center symmetry that can break down spontaneously. This happens at  $T_{RW}$ , where the system undergoes a second-order phase transition to a deconfined phase, where either of the two complex sectors can be selected, and the local Polyakov loops prefer to align to either  $e^{i\frac{2\pi}{3}}$  or  $e^{-i\frac{2\pi}{3}}$ . This opens a pseudogap of low spectral density in the Dirac spectrum, equal to the effective Matsubara frequency  $\omega_{RW} = (2\pi/3)T$ . According to the sea/islands picture (suitably adapted to the case of nonzero imaginary chemical potential), this pseudogap can be populated by localized modes living on the fluctuations of the Polyakov loop away from the ordered value. One then expects the low-lying Dirac modes to turn from delocalized to localized as  $T_{RW}$  is crossed. Confirming this scenario would lend more support to the conjectured strong connection between localization and deconfinement.

In this paper we study this scenario by means of numerical simulations on the lattice. In particular, we consider  $N_f = 2 + 1$  QCD with physical quark masses, discretized via improved staggered fermions, with a degenerate imaginary chemical potential coupled to all quark flavors, i.e., we consider a purely baryonic imaginary chemical potential. We then determine the localization temperature, at which the lowest modes turn from delocalized to localized, at finite spacing for different values  $N_t = 4, 6, 8$  of the temporal extension of the lattice. This is compared to the critical temperature of the Roberge-Weiss transition at the same  $N_t$ , as well as to its continuum extrapolation, obtained in Ref. [36] adopting the same discretization used in this study.

The paper is organized as follows. In Section II we provide details about the system discretization and the numerical algorithms adopted in our investigation; in Section III we discuss our numerical results; finally, in Section IV we draw our conclusions. Systematic effects on the determination of the mobility edge near the Roberge-Weiss transition are discussed in the Appendix.

## II. NUMERICAL SETUP

### A. Dirac spectrum and localization

The staggered operator at nonzero  $\hat{\mu}_I = \mu_I/T$  reads

$$(D_{\text{stag}}(\hat{\mu}_I))_{xy} = \frac{1}{2} \sum_{\alpha} \eta_{\alpha}(x) (e^{i\frac{\hat{\mu}_I}{N_t} \delta_{\alpha 4}} U_{\alpha}(x) \delta_{x+\hat{\alpha}y} - e^{-i\frac{\hat{\mu}_I}{N_t} \delta_{\alpha 4}} U_{\alpha}^{\dagger}(x - \hat{\alpha}) \delta_{x-\hat{\alpha}y}), \quad (1)$$

where  $U_{\alpha}(x) \in SU(3)$ ,  $\alpha = 1, \dots, 4$  are the link variables and  $\eta_{\alpha}(x)$  are the usual staggered phases. Periodic boundary conditions in the spatial directions, and antiperiodic boundary conditions in the temporal direction, are understood. The operator  $D_{\text{stag}}(\hat{\mu}_I)$  is anti-Hermitian and has the chiral property  $\{\eta_5, D_{\text{stag}}(\hat{\mu}_I)\} =$

0, where  $(\eta_5)_{xy} = \eta_5(x) \delta_{xy}$  with  $\eta_5(x) = (-1)^{\sum_{\alpha=1}^4 x_{\alpha}}$ . The spectrum of  $D_{\text{stag}}(\hat{\mu}_I)$  is purely imaginary due to anti-Hermiticity,

$$D_{\text{stag}}(\hat{\mu}_I)\psi_n = i\lambda_n\psi_n, \quad (2)$$

with  $\lambda_n \in \mathbb{R}$ , and furthermore symmetric with respect to zero thanks to the chiral property, since this implies  $D_{\text{stag}}(\hat{\mu}_I)\eta_5\psi_n = -i\lambda_n\eta_5\psi_n$ . This implies in particular that  $\det[D_{\text{stag}}(\hat{\mu}_I) + m]$  is real and positive.

The localization properties of the eigenmodes are determined by the large-volume scaling of the Inverse Participation Ratio (IPR), averaged over gauge configurations. The IPR is defined as:

$$\text{IPR}_n = \sum_x (\sum_c |(\psi_n(x))_c|^2)^2, \quad (3)$$

where  $c = 1, 2, 3$  is the color index. For modes effectively occupying a region of size  $V_{\text{eff}}$ , one finds  $\sum_c |(\psi_n(x))_c|^2 \sim 1/V_{\text{eff}}$  and so qualitatively  $\langle \text{IPR}_n \rangle \sim V_{\text{eff}}/V_{\text{eff}}^2 = 1/V_{\text{eff}}$ . Delocalized modes are extended all over the space, i.e.,  $V_{\text{eff}} \sim V$ , and so  $\langle \text{IPR}_n \rangle \sim 1/V \rightarrow 0$  as  $V \rightarrow \infty$ , while for localized modes  $V_{\text{eff}} \sim V_0$  is finite and  $V$ -independent, so that one expects  $\text{IPR}_n$  to remain constant as  $V \rightarrow \infty$ . Since  $\psi_n$  and  $\eta_5\psi_n$  have the same IPR, it suffices to focus on  $\lambda_n \geq 0$  only.

The localization properties of the eigenmodes  $\psi_n$  are most easily studied by exploiting their connection with the statistical properties of the spectrum [76]. In fact, localized modes are expected to fluctuate independently and so the corresponding eigenvalues are expected to obey Poisson statistics. For delocalized modes the corresponding eigenvalues are expected instead to obey the same statistics as the appropriate Gaussian ensemble of Random Matrix Theory (RMT) [77], once model-dependent features are removed by the unfolding procedure. For  $D_{\text{stag}}$  and  $SU(3)$  gauge fields, the right ensemble is the Gaussian unitary ensemble (GUE) [78]. The unfolded spectrum is defined by the mapping

$$x_n = \int^{\lambda_n} d\lambda' \rho(\lambda'), \quad (4)$$

where  $\rho(\lambda) = \langle \sum_n \delta(\lambda - \lambda_n) \rangle$  is the spectral density. In practice,  $x$  is the expected ranking of an eigenvalue equal to  $\lambda$  if this is found on a configuration. Convenient observables are obtained from the probability distribution  $p(s; \lambda)$  of the unfolded level spacings  $s_n = x_{n+1} - x_n$ , computed locally in the spectrum,

$$p(s; \lambda) = \frac{\langle \sum_n \delta(\lambda - \lambda_n) \delta(s - s_n) \rangle}{\langle \sum_n \delta(\lambda - \lambda_n) \rangle}. \quad (5)$$

For localized, independently fluctuating modes one expects  $p(s; \lambda)$  to be that corresponding to Poisson statistics,

$$p_{\text{Poisson}}(s) = e^{-s}, \quad (6)$$

while for delocalized modes  $p(s; \lambda)$  should be equal to that of the GUE, which is well approximated by the so-called Wigner surmise,

$$p_{\text{RMT}}(s) = \frac{32}{\pi^2} s^2 e^{-\frac{4}{\pi} s^2}. \quad (7)$$

The transition from localized to delocalized modes can be monitored by looking at how the features of  $p(s; \lambda)$  change across the spectrum. To this end, in this paper we have used the integrated probability distribution [79],

$$I_{s_0}(\lambda) = \int_0^{s_0} ds p(s; \lambda), \quad (8)$$

where  $s_0 \simeq 0.508$  is chosen to maximize the difference between Poisson and RMT-type statistics. For these statistics one finds  $I_{s_0, \text{Poisson}} \simeq 0.398$  and  $I_{s_0, \text{RMT}} \simeq 0.117$ . Moreover, the critical value at the mobility edge is known for this observable,  $I_{s_0, \text{crit}} = I_{s_0}(\lambda_c) = 0.1966(25)$  [57], and is expected to be universal. This can be used to identify the position of the mobility edge  $\lambda_c$  with good precision without the need for a finite-size scaling study, by simply looking at the crossing point of some interpolation of the numerical data and  $I_{s_0, \text{crit}}$ .

## B. Simulation details

We studied  $N_f = 2 + 1$  QCD on  $N_s^3 \times N_t$  hypercubic lattices using 2-stout improved [80] rooted staggered fermions with physical quark masses, at finite temperature  $T = 1/(aN_t)$  and in the presence of an imaginary chemical potential  $\mu_I$ . Gauge configurations were generated using a Rational Hybrid Monte-Carlo algorithm running on GPUs [81]. Details about the implementation can be found in Ref. [36]. For what follows it is useful to remember that the bare parameters, including the quark masses, are tuned so as to stay on a line of constant physics while changing the ultraviolet cut-off of the theory, following the determination reported in Refs. [82–84].

To study localization above the Roberge-Weiss point, we set  $\hat{\mu}_I = \pi$  and performed a scan in temperature at  $T > T_{\text{RW}}$ . We then computed the low modes of the staggered Dirac operator numerically using the ARPACK library [85]. We started using  $N_t = 4$  and doing a preliminary check for finite-volume effects, comparing the mobility edges obtained at a given temperature according to the procedure discussed above on lattices of increasing spatial dimension (this procedure is described in more detail in Sec. III). In particular, we used  $N_s = 24, 32, 40$  at  $T = 394 \text{ MeV}$  and  $N_s = 24, 32$  at  $T = 197 \text{ MeV}$ , finding in both cases compatible results for  $\lambda_c$  from the various volumes. This means that an aspect ratio  $r_{st} \equiv N_s/N_t = 24/4 = 6$  is expected to already reproduce well the thermodynamic limit. We then used also  $N_t = 6, 8$  to check for finite-spacing effects. Compatibly with the numerical effort, we used  $r_{st} = 8$  for  $N_t = 4$  and  $r_{st} = 6$  for  $N_t = 6, 8$ .

At  $\hat{\mu}_I = \pi$  the dynamics favors equally the two complex center sectors  $z = e^{\pm i\frac{2\pi}{3}}$  over the real sector  $z = 1$ . In the thermodynamic limit (taken in the presence of a suitable infinitesimal perturbation breaking the residual  $\mathbb{Z}_2$  symmetry) only one of the two complex sectors survives. In a finite volume, instead, the system tunnels between the two complex sectors (and with a much smaller probability, it can also tunnel to the real sector). For what concerns the staggered spectrum, however, one need not treat them separately to obtain the correct result in the thermodynamic limit. In fact, the spectrum of  $D_{\text{stag}}(\hat{\mu}_I = \pi) = D_{\text{stag}}^{\text{PBC}}$  (i.e., with periodic boundary condition in the temporal direction) on configuration  $U$  belonging to the center sector  $z$  is equal to the spectrum on configuration  $U^*$  belonging to the center sector  $z^*$ . If  $\lambda, \psi$  is an eigenpair on configuration  $U$ , one has

$$D_{\text{stag}}^{\text{PBC}}[U^*]\eta_5\psi^* = (-\eta_5 D_{\text{stag}}^{\text{PBC}}[U]\psi)^* = i\lambda\eta_5\psi^*. \quad (9)$$

In particular, this means that  $U$  and  $U^*$  have the same Boltzmann weight (in the absence of  $\mathbb{Z}_2$ -breaking perturbations). Any configuration belonging to the sector  $e^{-i\frac{2\pi}{3}}$  appearing in the simulation history can then be treated effectively as just another configuration in the sector  $e^{+i\frac{2\pi}{3}}$  (and viceversa), with the same spectrum, and with the correct weight if one restricted the configuration space to a single center sector (up to finite-size effects due to contaminations from the real sector). We have then not imposed any restriction on the configurations to be analyzed, and included them all in the analysis. Since we observed no tunnelling to the real sector in our simulation histories, the corresponding finite-size effects are absent.

## III. NUMERICAL RESULTS

### A. Determination of the mobility edge

To unfold the spectrum we collected all the eigenvalues in the ensemble of configurations obtained for a given lattice setup, ranked them by magnitude, and replaced them by their rank divided by the number of configurations. We then divided the spectrum in bins, and computed  $I_{s_0}(\lambda)$  in each bin separately, assigning the result to the central point of the bin. To ensure that bins are sufficiently small to reliably capture the local behavior of  $I_{s_0}(\lambda)$ , we have computed the average unfolded spacing  $\langle s \rangle_\lambda$  in each bin. This should equal 1, and we have checked that this is the case in the relevant spectral regions.<sup>1</sup>

<sup>1</sup> The relation  $\langle s \rangle_\lambda = 1$  follows from the fact that for infinite statistics and in the large-volume limit the average level spacing  $\langle \Delta \lambda \rangle_\lambda$  in an infinitesimal spectral region around  $\lambda$  equals  $1/\rho(\lambda)$ , and this is identically 1 for the unfolded spectrum by construction.

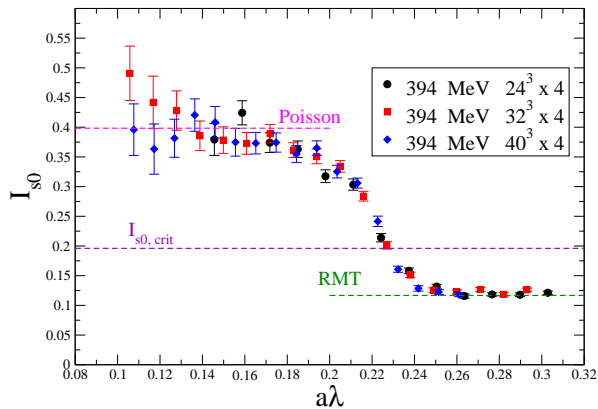


FIG. 1. Integrated probability distribution of the unfolded level spacings, computed locally in the spectrum, at  $T = 394$  MeV on  $N_s^3 \times 4$  lattices. Horizontal lines correspond to the expectation for Poisson statistics (corresponding to localized modes), RMT statistics (corresponding to delocalized modes), and critical statistics. An Anderson transition in the Dirac spectrum is found at the mobility edge where the curve intersects the critical value  $I_{s_0, \text{crit}}$ .

Results of this procedure are shown in Fig. 1, for  $T = 394$  MeV,  $N_t = 4$ , and the three different spatial volumes. The presence of localized modes at the low end of the spectrum is signalled by  $I_{s_0} \approx I_{s_0, \text{Poisson}}$ , while in the bulk  $I_{s_0} \approx I_{s_0, \text{RMT}}$  indicates that modes are delocalized. At the mobility edge  $\lambda_c$  where the Anderson transition from localized to delocalized modes takes place,  $I_{s_0}$  takes the critical value  $I_{s_0} = I_{s_0, \text{crit}}$ .

To determine  $\lambda_c$ , we constructed two cubic spline interpolations of  $I_{s_0} \pm \delta I_{s_0}$ , where  $\delta I_{s_0}$  is the statistical error on  $I_{s_0}$ , and looked for the crossing points of the spline interpolations with  $I_{s_0, \text{crit}}$ . We then determined  $\lambda_c$  as the average of the crossing points, with an associated error equal to the semi-dispersion. We also checked that changing the order of the spline interpolation leads to negligible effects on the determination of  $\lambda_c$ . The procedure is illustrated for  $T = 394$  MeV,  $N_t = 4$ , and the three different volumes in Fig. 2. Strictly speaking, the mobility edge is the point in the spectrum where  $I_{s_0}$  is volume-independent. Figure 2 shows that our procedure

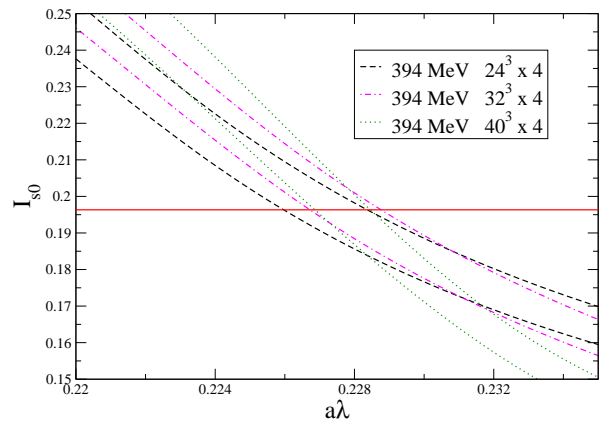


FIG. 2. Spline interpolations of  $I_{s_0} \pm \delta I_{s_0}$  used for the determination of the mobility edge. The horizontal line corresponds to  $I_{s_0, \text{crit}}$ , and its crossing points with the spline interpolations determine the error band for  $\lambda_c$ . Different spatial volumes yield consistent results.

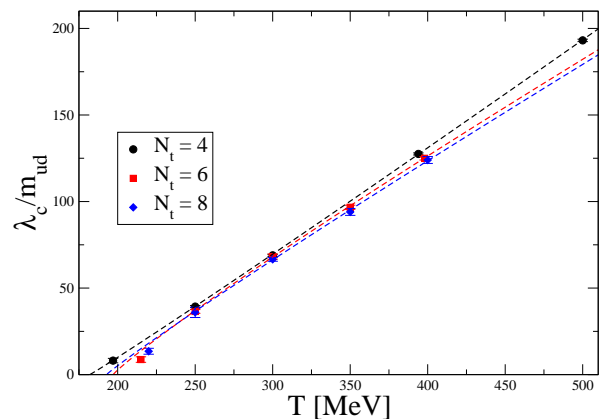


FIG. 3. Temperature dependence of the renormalized mobility edge. Dashed lines are best fits to the data at fixed  $N_t$  with the functional form Eq. (10), excluding the lowest temperature from each set.

yields consistent values for the three volumes, thus providing an accurate estimate for  $\lambda_c$ , and that statistical fluctuations dominate over the finite-size effects.

## B. Localization properties at the Roberge-Weiss phase transition

The results for the mobility edge, determined as discussed above, are collected in Fig. 3. There we show the renormalization-group-invariant ratio  $\tilde{\lambda}_c = \frac{\lambda_c}{m_{\text{ud}}}$ ,<sup>2</sup> with  $m_{\text{ud}}$  the bare light-quark mass, for all the temperatures

For finite statistics and volume one has necessarily to use sufficiently large finite bins in order to collect sufficiently many eigenvalues, and in regions where  $\rho(\lambda)$  is small the bin size may be comparable or even exceed the scale over which  $\rho(\lambda)$  varies appreciably. This leads to  $\rho(\lambda) \langle \Delta \lambda \rangle_\lambda \neq 1$  and in turn to  $\langle s \rangle_\lambda \neq 1$  in that region [65]. This happens in the lowest part of the staggered spectrum at high temperature where the spectral density is small. This region is problematic also due to the effects of the approximate taste symmetry of staggered fermions at finite lattice spacing, which distorts the spectral statistics from Poissonian [56, 86]. Moreover, since we computed a limited and fixed number of eigenvalues for each configuration, cut-off effects lead to  $\langle s \rangle_\lambda \neq 1$  also at the highest end of the spectral region being explored. However, both these spectral regions are irrelevant to our analysis and were discarded.

<sup>2</sup> Roughly speaking, the eigenvalues of the Dirac operator renormalize multiplicatively with the same renormalization constant as the quark mass [87, 88], and so is expected to do the mobility edge [56]. A proof that this is actually the case will be presented

$N_t$	$A$	$B$	$T_{\text{loc}} [\text{MeV}]$
4	0.51(1)	1.0(1)	183(4)
6	0.98(3)	0.91(5)	198(6)
8	0.8(4)	0.94(2)	193(10)

TABLE I. Coefficients of the best fit of the renormalized mobility edge to the functional form  $\tilde{\lambda}_c(T) = A(T - T_{\text{loc}})^B$ .

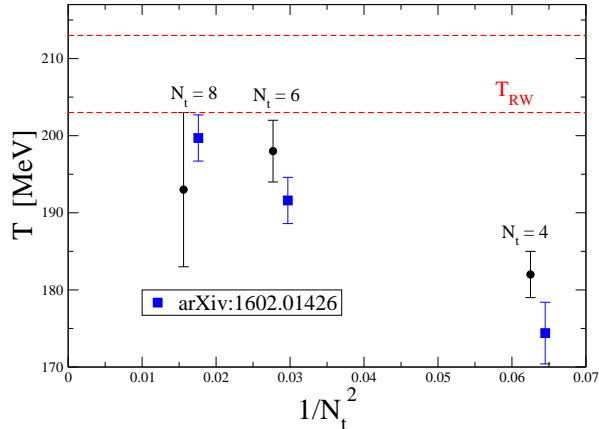


FIG. 4. Localization temperature  $T_{\text{loc}}(N_t)$ , where  $\tilde{\lambda}_c$  vanishes, for the various  $N_t$ s. For comparison, we show also the Roberge-Weiss temperatures  $T_{\text{RW}}(N_t)$  at finite spacing (slightly shifted horizontally) and the error band corresponding to its continuum extrapolation, obtained in Ref. [36].

and lattice spacings used in this work. The dependence on the lattice spacing is indeed mild, with  $\tilde{\lambda}_c(T, N_t)$  depending little on  $N_t$ .

It is evident that the mobility edge tends to vanish as  $T$  decreases toward  $T_{\text{RW}}$ . As the Roberge-Weiss transition, at least for  $N_f = 2 + 1$  QCD with physical quark masses and close enough to the continuum limit, is a continuous transition [36, 37], we also expect  $\tilde{\lambda}_c$  to vanish continuously. To leading order, we then expect

$$\tilde{\lambda}_c(T, N_t) = A(N_t) [T - T_{\text{loc}}(N_t)]^{B(N_t)}. \quad (10)$$

For each  $N_t$  we separately determined the localization temperature  $T_{\text{loc}}(N_t)$  where the mobility edge vanishes, by fitting the data to the functional form Eq. (10). In doing so, we have excluded the lowest temperature, closest to the transition, from each set. As we show in the Appendix, the determination of  $\lambda_c$  is still affected by systematic effects at the lowest temperature for the  $N_t = 6, 8$  ensembles, which could be due to finite size effects becoming more visible as the continuum limit is approached (see the Appendix for more details). Since this data point affects the outcome of the fit and may distort the result for

---

elsewhere [89]. Therefore, taking its ratio with the quark mass, which is tuned so as to stay on a line of constant physics, returns a renormalization-group invariant quantity.

$T_{\text{loc}}(N_t)$ , we have preferred to use only the more reliable results obtained at temperatures fairly and well above  $T_{\text{RW}}$ .

Results for  $T_{\text{loc}}(N_t)$  are shown in Fig. 4, together with the critical temperatures  $T_{\text{RW}}(N_t)$  at finite spacing and the band corresponding to the continuum-extrapolated result  $T_{\text{RW}} = 208(5)$  MeV for the Roberge-Weiss temperature, obtained in Ref. [36]. We find that  $T_{\text{loc}}(N_t)$  is compatible with  $T_{\text{RW}}(N_t)$  for all  $N_t$ s. A continuum extrapolation via a fit linear in  $1/N_t^2$  gives  $T_{\text{loc}} = 204(7)$  MeV, in good agreement with  $T_{\text{RW}}$ .

#### IV. CONCLUSIONS

We have studied the localization properties of the low-lying modes of the staggered operator at imaginary chemical potential  $\mu_I/T = \pi$  in  $N_f = 2 + 1$  QCD above the Roberge-Weiss temperature  $T_{\text{RW}}$ , by means of numerical lattice simulations with rooted staggered fermions at physical quark masses. We found that the low modes are localized up to a temperature- and spacing-dependent mobility edge  $\lambda_c$ , that is extrapolated to vanish at  $T_{\text{loc}}(N_t)$ . For the renormalized mobility edge  $\lambda_c/m_{\text{ud}}$ , and sufficiently above  $T_{\text{RW}}$ , we observed only a mild dependence on  $N_t$ , as expected. For the localization temperatures  $T_{\text{loc}}(N_t)$  where the mobility edge vanishes for the various  $N_t$ s we obtained values in agreement with the determination of the critical temperatures  $T_{\text{RW}}(N_t)$  of Ref. [36]. The same is true for their continuum extrapolations. This supports the expectation that localized modes appear precisely at the deconfinement transition of a gauge theory, when such a transition is sharp. In particular, this is the first case when the close connection between localization of the low Dirac modes and deconfinement is demonstrated for a genuine deconfinement transition in the presence of dynamical fermions that survives the continuum limit.

#### Appendix A: Systematic effects near $T_{\text{RW}}$

$N_t$	$T_{\text{min}} [\text{MeV}]$	$T_{\text{loc}} [\text{MeV}]$	$T_{\text{loc}} [\text{MeV}]$
		( $T_{\text{min}}$ excluded)	( $T_{\text{min}}$ included)
4	197	183(4)	183(2)
6	215	198(6)	206(2)
8	220	193(10)	205(3)

TABLE II.  $T_{\text{loc}}$  obtained from fits excluding or including the lowest temperature  $T_{\text{min}}$  for the various  $N_t$ .

To further check for finite-size and other systematic effects near the transition, for each  $N_t$  we compared the results of fits to  $\tilde{\lambda}_c(T, N_t)$  performed including or excluding the lowest temperature from each set. The temperature closest to the Roberge-Weiss transition is in fact the one

affected the most by finite-size effects due to the larger correlation length. In particular, taste-violating effects become milder as the lattice becomes finer, leading to the formation of multiplets of low modes that distort the spectral statistics. This can affect our determination of the mobility edge when this is close to zero, especially on our finer  $N_t = 6, 8$  ensembles.

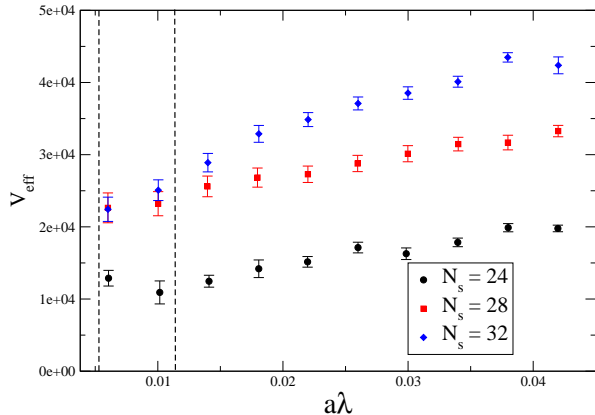


FIG. 5. Size  $V_{\text{eff}} = \text{IPR}^{-1}$  of low modes on  $N_t = 6$  lattices at  $T = 200$  MeV for  $V = N_s^3 = 24^3, 28^3, 32^3$ . For the lowest modes  $a\lambda \lesssim 0.01$  this is approximately the same for the two largest volumes, indicating that they are localized.

It is already evident from Fig. (3) that including the lowest temperature in a fit of the form Eq. (10) will alter the result for  $T_{\text{loc}}(N_t = 6, 8)$ . The results are reported in Tab. II. For  $N_t = 4$  the two results are compatible: this is not surprising, given the relative coarseness of the lattice and the larger aspect ratio. For  $N_t = 6$  and  $N_t = 8$ , instead, the difference is substantial, and around 4% and 6%, respectively.

To show explicitly that the determination of  $T_{\text{loc}}(N_t = 6)$  is inaccurate if the lowest temperature  $T = 215$  MeV is included, we have done a short run at  $T = 200$  MeV on three volumes,  $N_s = 24, 28, 32$ . Below  $a\lambda \simeq 0.01$  the size of the modes,  $V_{\text{eff}} = \text{IPR}^{-1}$ , is compatible within  $1\sigma$  for the  $N_s = 28, 32$  ensembles (see Fig. 5). This is a clear indication that the lowest modes are localized, and so that necessarily  $T_{\text{loc}}(N_t = 6) < 200$  MeV. We take this as an indication that our sample of  $N_t = 6$  configurations at  $T = 215$  MeV is affected by strong systematic effects, which are likely a combination of finite-size effects and limited statistics. Instead, the value obtained excluding the lowest temperature is compatible with this finding.

*Acknowledgments* We thank G. Clemente and F. Sanfilippo for helping implement the diagonalization code. Numerical simulations have been performed on the MARCONI and MARCONI100 machines at CINECA, based on the agreement between INFN and CINECA (under projects INF20 npqcd, INF21 npqcd). M. G. is partially supported by the NKFIH grant KKP-126769.

- 
- [1] P. de Forcrand and O. Philipsen, Nucl. Phys. B **642**, 290 (2002), arXiv:hep-lat/0205016 [hep-lat].
- [2] M. D’Elia and M. P. Lombardo, Phys. Rev. D **67**, 014505 (2003), arXiv:hep-lat/0209146 [hep-lat].
- [3] M. D’Elia and F. Sanfilippo, Phys. Rev. D **80**, 014502 (2009), arXiv:0904.1400 [hep-lat].
- [4] P. Cea, L. Cosmai, M. D’Elia, and A. Papa, J. High Energy Phys. **02**, 066 (2007), arXiv:hep-lat/0612018.
- [5] P. Cea, L. Cosmai, and A. Papa, Phys. Rev. D **89**, 074512 (2014), arXiv:1403.0821 [hep-lat].
- [6] C. Bonati, P. de Forcrand, M. D’Elia, O. Philipsen, and F. Sanfilippo, Phys. Rev. D **90**, 074030 (2014), arXiv:1408.5086 [hep-lat].
- [7] P. Cea, L. Cosmai, and A. Papa, Phys. Rev. D **93**, 014507 (2016), arXiv:1508.07599 [hep-lat].
- [8] C. Bonati, M. D’Elia, M. Mariti, M. Mesiti, F. Negro, and F. Sanfilippo, Phys. Rev. D **92**, 054503 (2015), arXiv:1507.03571 [hep-lat].
- [9] R. Bellwied, S. Borsányi, Z. Fodor, J. Günther, S. D. Katz, C. Ratti, and K. K. Szabó, Phys. Lett. B **751**, 559 (2015), arXiv:1507.07510 [hep-lat].
- [10] M. D’Elia, G. Gagliardi, and F. Sanfilippo, Phys. Rev. D **95**, 094503 (2017), arXiv:1611.08285 [hep-lat].
- [11] J. N. Günther, R. Bellwied, S. Borsányi, Z. Fodor, S. D. Katz, A. Pásztor, C. Ratti, and K. K. Szabó, Nucl. Phys. A **967**, 720 (2017), arXiv:1607.02493 [hep-lat].
- [12] P. Alba *et al.*, Phys. Rev. D **96**, 034517 (2017), arXiv:1702.01113 [hep-lat].
- [13] V. Vovchenko, A. Pásztor, Z. Fodor, S. D. Katz, and H. Stoecker, Phys. Lett. B **775**, 71 (2017), arXiv:1708.02852 [hep-ph].
- [14] C. Bonati, M. D’Elia, F. Negro, F. Sanfilippo, and K. Zambello, Phys. Rev. D **98**, 054510 (2018), arXiv:1805.02960 [hep-lat].
- [15] S. Borsányi, Z. Fodor, J. N. Günther, S. K. Katz, K. K. Szabó, A. Pásztor, I. Portillo, and C. Ratti, J. High Energy Phys. **10**, 205 (2018), arXiv:1805.04445 [hep-lat].
- [16] R. Bellwied, S. Borsányi, Z. Fodor, J. N. Günther, J. Noronha-Hostler, P. Parotto, A. Pásztor, C. Ratti, and J. M. Stafford, Phys. Rev. D **101**, 034506 (2020), arXiv:1910.14592 [hep-lat].
- [17] S. Borsányi, Z. Fodor, J. N. Günther, R. Kara, S. D. Katz, P. Parotto, A. Pásztor, C. Ratti, and K. K. Szabó, Phys. Rev. Lett. **125**, 052001 (2020), arXiv:2002.02821 [hep-lat].

- [18] A. Roberge and N. Weiss, Nucl. Phys. B **275**, 734 (1986).
- [19] M. D’Elia, F. Di Renzo, and M. P. Lombardo, Phys. Rev. D **76**, 114509 (2007), arXiv:0705.3814 [hep-lat].
- [20] P. Cea, L. Cosmai, M. D’Elia, C. Manneschi, and A. Papa, Phys. Rev. D **80**, 034501 (2009), arXiv:0905.1292 [hep-lat].
- [21] M. D’Elia and F. Sanfilippo, Phys. Rev. D **80**, 111501 (2009), arXiv:0909.0254 [hep-lat].
- [22] C. Bonati, G. Cossu, M. D’Elia, and F. Sanfilippo, Phys. Rev. D **83**, 054505 (2011), arXiv:1011.4515 [hep-lat].
- [23] P. de Forcrand and O. Philipsen, Phys. Rev. Lett. **105**, 152001 (2010), arXiv:1004.3144 [hep-lat].
- [24] P. Cea, L. Cosmai, M. D’Elia, A. Papa, and F. Sanfilippo, Phys. Rev. D **85**, 094512 (2012), arXiv:1202.5700 [hep-lat].
- [25] O. Philipsen and C. Pinke, Phys. Rev. D **89**, 094504 (2014), arXiv:1402.0838 [hep-lat].
- [26] A. Alexandru and A. Li, PoS **LATTICE2013**, 208 (2014), arXiv:1312.1201 [hep-lat].
- [27] L.-K. Wu and X.-F. Meng, Phys. Rev. D **87**, 094508 (2013), arXiv:1303.0336 [hep-lat].
- [28] L.-K. Wu and X.-F. Meng, Phys. Rev. D **90**, 094506 (2014), arXiv:1405.2425 [hep-lat].
- [29] L.-K. Wu and X.-F. Meng, Phys. Rev. D **95**, 054503 (2017), arXiv:1612.03384 [hep-lat].
- [30] K. Nagata, K. Kashiwa, A. Nakamura, and S. M. Nishigaki, Phys. Rev. D **91**, 094507 (2015), arXiv:1410.0783 [hep-lat].
- [31] T. Makiyama, Y. Sakai, T. Saito, M. Ishii, J. Takahashi, K. Kashiwa, H. Kouno, A. Nakamura, and M. Yahiro, Phys. Rev. D **93**, 014505 (2016), arXiv:1502.06191 [hep-lat].
- [32] C. Czaban, F. Cuteri, O. Philipsen, C. Pinke, and A. Sciarra, Phys. Rev. D **93**, 054507 (2016), arXiv:1512.07180 [hep-lat].
- [33] C. Pinke and O. Philipsen, PoS **LATTICE2015**, 149 (2016), arXiv:1508.07725 [hep-lat].
- [34] K. Kashiwa and A. Ohnishi, Phys. Rev. D **93**, 116002 (2016), arXiv:1602.06037 [hep-ph].
- [35] K. Kashiwa and A. Ohnishi, Phys. Lett. B **750**, 282 (2015), arXiv:1505.06799 [hep-ph].
- [36] C. Bonati, M. D’Elia, M. Mariti, M. Mesiti, F. Negro, and F. Sanfilippo, Phys. Rev. D **93**, 074504 (2016), arXiv:1602.01426 [hep-lat].
- [37] C. Bonati, E. Calore, M. D’Elia, M. Mesiti, F. Negro, F. Sanfilippo, S. F. Schifano, G. Silvi, and R. Tripiccione, Phys. Rev. D **99**, 014502 (2019), arXiv:1807.02106 [hep-lat].
- [38] H. Kouno, Y. Sakai, K. Kashiwa, and M. Yahiro, J. Phys. G **36**, 115010 (2009), arXiv:0904.0925 [hep-ph].
- [39] Y. Sakai, K. Kashiwa, H. Kouno, M. Matsuzaki, and M. Yahiro, Phys. Rev. D **79**, 096001 (2009), arXiv:0902.0487 [hep-ph].
- [40] Y. Sakai, T. Sasaki, H. Kouno, and M. Yahiro, Phys. Rev. D **82**, 076003 (2010), arXiv:1006.3648 [hep-ph].
- [41] T. Sasaki, Y. Sakai, H. Kouno, and M. Yahiro, Phys. Rev. D **84**, 091901 (2011), arXiv:1105.3959 [hep-ph].
- [42] H. Kouno, M. Kishikawa, T. Sasaki, Y. Sakai, and M. Yahiro, Phys. Rev. D **85**, 016001 (2012), arXiv:1110.5187 [hep-ph].
- [43] G. Aarts, S. P. Kumar, and J. Rafferty, J. High Energy Phys. **07**, 056 (2010), arXiv:1005.2947 [hep-th].
- [44] J. Rafferty, J. High Energy Phys. **09**, 087 (2011), arXiv:1103.2315 [hep-th].
- [45] K. Morita, V. Skokov, B. Friman, and K. Redlich, Phys. Rev. D **84**, 076009 (2011), arXiv:1107.2273 [hep-ph].
- [46] K. Kashiwa, T. Hell, and W. Weise, Phys. Rev. D **84**, 056010 (2011), arXiv:1106.5025 [hep-ph].
- [47] V. Pagura, D. Gómez Dumm, and N. N. Scoccola, Phys. Lett. B **707**, 76 (2012), arXiv:1105.1739 [hep-ph].
- [48] D. Scheffler, M. Buballa, and J. Wambach, Acta Phys. Polon. Supp. **5**, 971 (2012), arXiv:1111.3839 [hep-ph].
- [49] K. Kashiwa and R. D. Pisarski, Phys. Rev. D **87**, 096009 (2013), arXiv:1301.5344 [hep-ph].
- [50] K. Kashiwa, T. Sasaki, H. Kouno, and M. Yahiro, Phys. Rev. D **87**, 016015 (2013), arXiv:1208.2283 [hep-ph].
- [51] M. Giordano and T. G. Kovács, Universe **7**, 194 (2021), arXiv:2104.14388 [hep-lat].
- [52] A. M. García-García and J. C. Osborn, Nucl. Phys. **A770**, 141 (2006), arXiv:hep-lat/0512025 [hep-lat].
- [53] A. M. García-García and J. C. Osborn, Phys. Rev. D **75**, 034503 (2007), arXiv:hep-lat/0611019 [hep-lat].
- [54] T. G. Kovács, Phys. Rev. Lett. **104**, 031601 (2010), arXiv:0906.5373 [hep-lat].
- [55] T. G. Kovács and F. Pittler, Phys. Rev. Lett. **105**, 192001 (2010), arXiv:1006.1205 [hep-lat].
- [56] T. G. Kovács and F. Pittler, Phys. Rev. D **86**, 114515 (2012), arXiv:1208.3475 [hep-lat].
- [57] M. Giordano, T. G. Kovács, and F. Pittler, Phys. Rev. Lett. **112**, 102002 (2014), arXiv:1312.1179 [hep-lat].
- [58] S. M. Nishigaki, M. Giordano, T. G. Kovács, and F. Pittler, PoS **LATTICE2013**, 018 (2014), arXiv:1312.3286 [hep-lat].
- [59] M. Giordano, T. G. Kovács, and F. Pittler, Int. J. Mod. Phys. **A29**, 1445005 (2014), arXiv:1409.5210 [hep-lat].
- [60] L. Ujjalusi, M. Giordano, F. Pittler, T. G. Kovács, and I. Varga, Phys. Rev. D **92**, 094513 (2015), arXiv:1507.02162 [cond-mat.dis-nn].
- [61] M. Giordano, S. D. Katz, T. G. Kovács, and F. Pittler, J. High Energy Phys. **02**, 055 (2017),



- arXiv:1611.03284 [hep-lat].
- [62] G. Cossu and S. Hashimoto, *J. High Energy Phys.* **06**, 056 (2016), arXiv:1604.00768 [hep-lat].
- [63] L. Holicki, E.-M. Ilgenfritz, and L. von Smekal, *PoS LATTICE2018*, 180 (2018), arXiv:1810.01130 [hep-lat].
- [64] T. G. Kovács and R. Á. Vig, *Phys. Rev. D* **97**, 014502 (2018), arXiv:1706.03562 [hep-lat].
- [65] M. Giordano, *J. High Energy Phys.* **05**, 204 (2019), arXiv:1903.04983 [hep-lat].
- [66] R. Á. Vig and T. G. Kovács, *Phys. Rev. D* **101**, 094511 (2020), arXiv:2001.06872 [hep-lat].
- [67] C. Bonati, M. Cardinali, M. D’Elia, M. Giordano, and F. Mazzioni, *Phys. Rev. D* **103**, 034506 (2021), arXiv:2012.13246 [hep-lat].
- [68] G. Baranka and M. Giordano, *Phys. Rev. D* **104**, 054513 (2021), arXiv:2104.03779 [hep-lat].
- [69] F. Bruckmann, T. G. Kovács, and S. Schierenberg, *Phys. Rev. D* **84**, 034505 (2011), arXiv:1105.5336 [hep-lat].
- [70] M. Giordano, T. G. Kovács, and F. Pittler, *J. High Energy Phys.* **04**, 112 (2015), arXiv:1502.02532 [hep-lat].
- [71] M. Giordano, T. G. Kovács, and F. Pittler, *J. High Energy Phys.* **06**, 007 (2016), arXiv:1603.09548 [hep-lat].
- [72] M. Giordano, T. G. Kovács, and F. Pittler, *Phys. Rev. D* **95**, 074503 (2017), arXiv:1612.05059 [hep-lat].
- [73] F. Karsch, E. Laermann, and C. Schmidt, *Phys. Lett. B* **520**, 41 (2001), arXiv:hep-lat/0107020 [hep-lat].
- [74] P. de Forcrand and O. Philipsen, *Nucl. Phys.* **B673**, 170 (2003), arXiv:hep-lat/0307020 [hep-lat].
- [75] P. de Forcrand and O. Philipsen, *J. High Energy Phys.* **11**, 012 (2008), arXiv:0808.1096 [hep-lat].
- [76] B. L. Altshuler and B. I. Shklovskii, *Sov. Phys. JETP* **64**, 127 (1986).
- [77] M. L. Mehta, *Random matrices*, 3rd ed., Vol. 142 (Elsevier, 2004).
- [78] J. J. M. Verbaarschot and T. Wettig, *Ann. Rev. Nucl. Part. Sci.* **50**, 343 (2000), arXiv:hep-ph/0003017 [hep-ph].
- [79] B. I. Shklovskii, B. Shapiro, B. R. Sears, P. Lambrianides, and H. B. Shore, *Phys. Rev. B* **47**, 11487 (1993).
- [80] C. Morningstar and M. J. Peardon, *Phys. Rev. D* **69**, 054501 (2004), arXiv:hep-lat/0311018.
- [81] C. Bonati, E. Calore, M. D’Elia, M. Mesiti, F. Negro, F. Sanfilippo, S. F. Schifano, G. Silvi, and R. Tripiccion, *Int. J. Mod. Phys. C* **29**, 1850010 (2018), arXiv:1801.01473 [hep-lat].
- [82] Y. Aoki, S. Borsányi, S. Dürr, Z. Fodor, S. D. Katz, S. Krieg, and K. K. Szabó, *J. High Energy Phys.* **06**, 088 (2009), arXiv:0903.4155 [hep-lat].
- [83] S. Borsányi, G. Endrődi, Z. Fodor, A. Jakovác, S. D. Katz, S. Krieg, C. Ratti, and K. K. Szabó, *J. High Energy Phys.* **11**, 077 (2010), arXiv:1007.2580 [hep-lat].
- [84] S. Borsányi, Z. Fodor, C. Hoelbling, S. D. Katz, S. Krieg, and K. K. Szabó, *Phys. Lett. B* **730**, 99 (2014), arXiv:1309.5258 [hep-lat].
- [85] R. B. Lehoucq, D. C. Sorensen, and C. Yang, *ARPACK users’ guide: solution of large-scale eigenvalue problems with implicitly restarted Arnoldi methods* (SIAM, 1998).
- [86] T. G. Kovács and F. Pittler, *PoS LATTICE2011*, 213 (2011), arXiv:1111.3524 [hep-lat].
- [87] L. Del Debbio, L. Giusti, M. Lüscher, R. Petronzio, and N. Tantalò, *J. High Energy Phys.* **02**, 011 (2006), arXiv:hep-lat/0512021.
- [88] L. Giusti and M. Lüscher, *J. High Energy Phys.* **03**, 013 (2009), arXiv:0812.3638 [hep-lat].
- [89] M. Giordano (2021), in preparation.